Title
Inorganic A-site cations improve the performance of band-edge carriers in lead halide perovskites.

Journal
Frontiers of Optoelectronics, 16(1)

Authors
Rong, Yaoguang
Wang, Ti
Wang, Cheng

Publication Date
2023-09-25

DOI
10.1007/s12200-023-00078-z

Peer reviewed

Frontiers of Optoelectronics (2023) 16:25
https://doi.org/10.1007/s12200-023-00078-z

Frontiers of Optoelectronics

RESEARCH ARTICLE

Inorganic A-site cations improve the performance of band-edge carriers in lead halide perovskites

Cheng Wang[1] · Yaoguang Rong[2] · Ti Wang[1]

Received: 28 April 2023 / Accepted: 17 July 2023

Abstract
In lead halide perovskites, organic A-site cations are generally introduced to fine-tune the properties. One of the questions under debate is whether organic A-site cations are essential for high-performance solar cells. In this study, we compare the band edge carrier dynamics and diffusion process in $MAPbBr_3$ and $CsPbBr_3$ single-crystal microplates. By transient absorption microscopy, the band-edge carrier diffusion constants are unraveled. With the replacement of inorganic A-site cations, the diffusion constant in $CsPbBr_3$ increases almost 8 times compared to that in $MAPbBr_3$. This work reveals that introducing inorganic A-site cations can lead to a much larger diffusion length and improve the performance of band-edge carriers.

Keywords Perovskite · Inorganic cations · Carrier diffusion

1 Introduction

With a typical chemical formulation of ABX_3, lead halide perovskites (LHP) have been demonstrated as promising semiconductors due to their remarkable optoelectronic properties, including long carrier lifetime, long diffusion length, high absorption coefficient, and photoluminescence (PL) efficiencies [1–4]. With these outstanding features, tremendous efforts have been made to fabricate LHP-based devices, such as light-emitting diodes, lasers, and solar cells [5–8]. Notably, the conversion efficiency records for solar cells are continually being refreshed, leaping from 3.8% in 2009 to 25.8% recently [9, 10]. During this development, the A cations of the LHP have been limited to methylammonium (MA^+), formamidinium (FA^+), and cesium (Cs^+) due to the tolerance factor. In conventional thoughts, the A-site cations cannot directly contribute to the LHP band-edge and hardly affect the optoelectronic properties [11–13]. However, some studies have proposed that fast motions of A-site cations are responsible for carrier trapping and electron–hole recombination [14–16]. In addition, polar methylammonium organic cations have been demonstrated to have the ability to detune state coupling and extend hot carrier lifetime [17]. Moreover, fine-tuning of A-site cations is an effective way to improve the structure stability, which is essential for the industrialization of LHP-based devices [18]. For example, inorganic cesium lead perovskite ($CsPbX_3$) has better tolerance of humidity, temperature, light, and voltage [19–21]. Although the stability of the materials has been improved with inorganic A-site cations, it is still unclear how inorganic A-site cations impact the carrier transport as well as the device performance in LHP.

Recently, perovskite single-crystal nanostructures have attracted attention owing to their advantages in size and optoelectronic properties [8, 22]. Traditional techniques, such as the Hall effect, time-of-flight, and PL quenching, have limitations in revealing carrier transport properties in an individual nanostructure perovskite [3, 23, 24]. Tian et al. used time-resolved and PL-scanned imaging microscopy to illustrate the carrier diffusion process in nanowire and nanoplate perovskites [25]. Hu et al. investigated the electric field-modulated PL imaging method to study the carrier transport in perovskite nanoplates [26]. However, these two techniques need a vigorous PL intensity from samples to achieve a high signal-to-noise ratio. Recently, transient absorption microscopy (TAM) has been demonstrated to be an efficient way to directly visualize the carrier diffusion

✉ Ti Wang
wangti@whu.edu.cn

1 Key Laboratory of Artificial Micro- and Nano-Structures of Ministry of Education, School of Physics and Technology, Wuhan University, Wuhan 430072, China

2 Wuhan National Laboratory for Optoelectronics, Huazhong University of Science and Technology, Wuhan 430074, China

Published online: 25 September 2023

process, and many studies have been carried out on organic materials, 2D materials, and perovskites [27–29]. To answer the questions whether inorganic cations are essential to the performance of lead halide perovskites, here we investigate the band edge carrier dynamics and diffusion process of $MAPbBr_3$ and $CsPbBr_3$ single crystal microplates. With the replacement of inorganic Cs^+ cations, $CsPbBr_3$ presents faster bulk recombination dynamics and a larger diffusion constant for the band edge carriers. Due to the high improvement of diffusion constant, the calculated diffusion length of $CsPbBr_3$ band edge carrier is much larger than that of $MAPbBr_3$. This work highlights that introducing inorganic Cs^+ cations can benefit the carrier extraction and may achieve excellent photovoltaic performances.

2 Experimental

The synthesis of $MAPbBr_3$ and $CsPbBr_3$ microplates followed our previously reported methods [30, 31]. Specifically, the $MAPbBr_3$ microplates were synthesized by immersing a $PbAc_2$-coated glass slide in a 7 mg/mL MABr solution in isopropanol at room temperature (22 °C) for about one day, with the $PbAc_2$ coated side facing down. The $PbAc_2$ thin film was prepared by drop-casting 100 mg/mL $PbAc_2{\cdot}3H_2O$ aqueous solution on a glass slide and dried at 60 °C. The $CsPbBr_3$ microplates were synthesized in a home-built chemical vapor deposition system. The ground powders of CsBr and $PbBr_2$ (molar ratio 1:1) were mixed and used as precursors for $CsPbBr_3$ and placed at the center of the heating zone. Phlogopite mica $[KMg_3(AlSi_3O_{10})F_2]$ was used as a growth substrate and placed downstream of the cooling area. The Argon gas was used as the carrier with a flow rate of 12 sccm and the pressure inside the tube was maintained at 80 mTorr. The center of the heating zone was set to 350 °C and the growth time was ~1 h. Note that the growth condition tended to yield more $CsPbBr_3$ microwires than $CsPbBr_3$ microplates on the substrate. Optical images of $MaPbBr_3$ and $CsPbBr_3$ microplates are shown in supplementary materials (Fig. S1).

Transient absorption (TA) spectra of perovskite films were measured by a femtosecond pump-probe system with a home-built TA spectrometer. Laser pulses at 1030 nm with 250 fs duration were generated by a 400 kHz amplified Yb:KGW laser system (PHAROS, Light Conversion Ltd.). The probe beam was a white light continuum beam spanning a 450 to 950 nm spectral region, created by focusing 5% of the 1030 nm fundamental output onto a YAG crystal.

A home-built TAM system was used to measure the carrier diffusion process. Briefly, the output of a high-repetition-rate amplifier (Pharos Light Conversion, 400 kHz, 1030 nm) pumped two independent optical parametric amplifiers (TOPAS-Twins, Light Conversion Ltd.). A mechanical translation stage (Thorlabs, DDS600-E) was used to delay the. Both the pump and probe beams were focused onto the samples by an objective (CFI Apo TIRF, Nikon Inc., 60×, NA 1.40). The probe beam was collected by another objective and was detected by an avalanche photodiode (APD; Hamamatsu, C5331-04). A lock-in amplifier was used to identify the change in the probe transmission (ΔT) induced by the pump. A pair of Galvanometer mirrors (Thorlabs GVS012) was used to scan the probe beam relative to the pump beam in space to obtain the carrier propagation images.

3 Results and discussion

Figure 1a shows the PL spectra of $CsPbBr_3$ and $MAPbBr_3$. The peak positions of $CsPbBr_3$ and $MAPbBr_3$ are at 520 and 538 nm, respectively. Although theoretical studies have illustrated that the valence and conduction bands of $APbX_3$ are

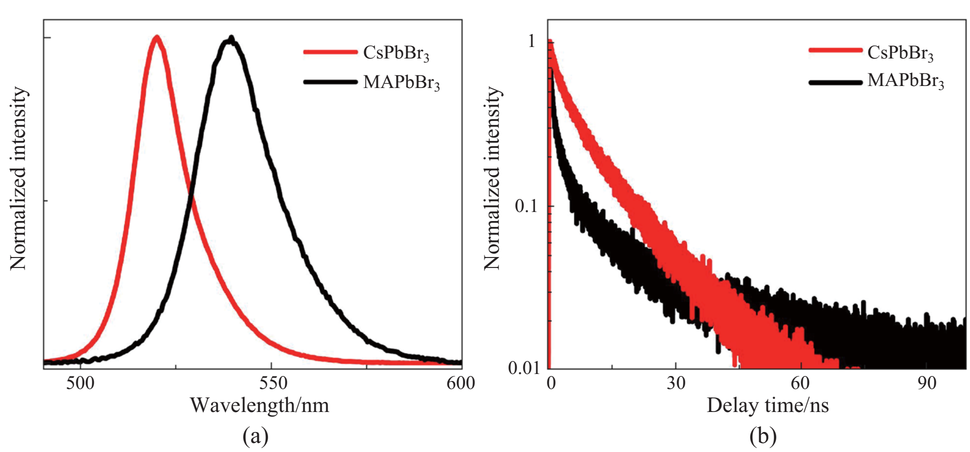

Fig. 1 Optical properties of $MAPbBr_3$ and $CsPbBr_3$ as determined in this study. **a** PL spectra. **b** TRPL. The excitation wavelength is 400 nm

dominated by contributions from the PbX_3^- inorganic sublattice, the A-site cation can fine-tune the lattice parameter and then affect the band gap. As the Cs^+ cation has a smaller size than the MA^+ cation, the lattice parameter of $CsPbBr_3$ should be smaller than that of $MAPbBr_3$. According to band theory, the smaller lattice parameter has a larger band gap, which is consistent with our PL spectra. This subtle difference between the two band gaps has also been demonstrated by experimental and theoretical analysis [32]. Moreover, the full width at half maximum (FWHM) of $CsPbBr_3$ is smaller than that of $MAPbBr_3$. The broadening of PL in LHP is dominated by trap emission. Smaller FWHM indicates that the trap-assisted nonradiative surface recombination in $CsPbBr_3$ is suppressed.

To study the carrier decay dynamics, time-resolved PL (TRPL) kinetics are presented in Fig. 1b. Both the dynamics of $MAPbBr_3$ and $CsPbBr_3$ fit a bi-exponential decay function. For $MAPbBr_3$, a short lifetime of around 1.3 ns and a longer one of around 13.7 ns were observed. $CsPbBr_3$ has a shorter lifetime of around 2.4 ns and a longer one of about 11.9 ns. Surface recombination effects have previously been observed in single-crystal perovskite materials [33]. The fast decay is attributed to surface recombination at the surface. However, the surface recombination rate for $MAPbBr_3$ was found in the present study to be much faster than that of $CsPbBr_3$. This difference may have been caused by the growth method. The CVD growth of $CsPbBr_3$ induced fewer defects at the surface. This result is consistent with the PL broadening mentioned above. However, for the $MAPbBr_3$, the solution process brought in more surface defects. Excluding the surface recombination process, the slow decay can be attributed to the bulk-free carrier. Previous theoretical work has shown that the electron–hole recombination behavior of $MAPbBr_3$ is slower than that of $CsPbBr_3$. They conclude that the A-site cation plays a significant role in determining the excited-state lifetime by influencing the nonadiabatic electron–phonon coupling. Thus, the observation here is consistent with the theoretical kinetics.

To further study the effects of the A-site cation on the dynamics, TA spectroscopy was performed. Figure 2a, c

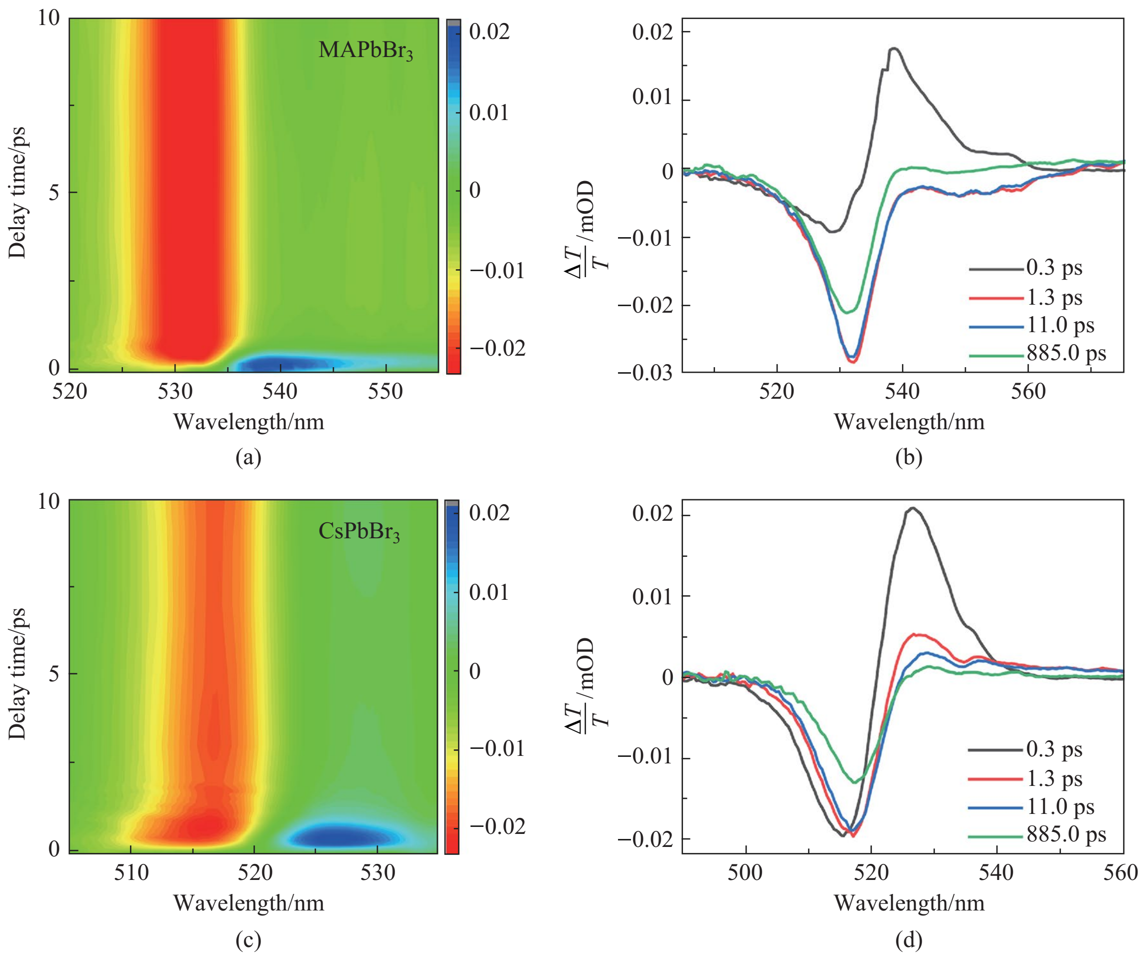

Fig. 2 Carrier dynamics of $MAPbBr_3$ and $CsPbBr_3$. **a** Pseudo TA color image of $MAPbBr_3$. **b** TA spectra of $MAPbBr_3$ at various delay time. **c** Pseudo TA color image of $CsPbBr_3$. **d** TA spectra of $CsPbBr_3$ at various delay time. The excitation wavelength is 400 nm

show the ensemble broadband TA image in pseudo-color plots at early delay time. For both $MAPbBr_3$ and $CsPbBr_3$, the excitation wavelength was 400 nm. Upon photoexcitation, a ground state bleach band (GSB, the negative signal in $\Delta T/T$, and ΔT is a pump-induced change in probe transmission, and T is the probe transmission) centered around the bandgap at 530 nm was observed due to the band-filling effect for $MAPbBr_3$. A photoinduced absorption (PIA, positive signal in $\Delta T/T$) band near 537 nm was observed at a delay time shorter than 1 ps (Fig. 2b). Previous works have demonstrated that this PIA peak is related to hot carriers [34]. The TA spectra of $CsPbBr_3$ showed similar features to those of $MAPbBr_3$, where the GSB and PIA peaks were measured to be at 517 and 526 nm, respectively. The GSB dynamics of $MAPbBr_3$ and $CsPbBr_3$ were found to be very similar (Fig. S2). For the TA measurements, the transmission mode was applied. The signal was the transmission light after samples, which reflected the features of the bulk sample. However, the reflection mode was used for the TRPL measurements which were more sensitive to the surface. Moreover, since the TRPL dynamics of $MAPbBr_3$ was slower than that of $CsPbBr_3$, the similar GSB dynamics indicated a faster nonradiative recombination process in $MAPbBr_3$.

TAM measurements have previously been demonstrated as an efficient technique to study the carrier diffusion process which can directly visualize the carrier distribution in materials. To analyze the band edge carrier diffusion in these microplates, the pump wavelength was selected at 400 nm for both perovskite materials. The probe wavelengths for $MAPbBr_3$ and $CsPbBr_3$ were selected for 530 and 517 nm respectively, which were the GSB peaks related to the band edge carrier. Perovskite materials show up to hundreds of ps lifetime of hot carriers due to the hot-phonon bottleneck effect with excitation density higher than 10^{18} cm^{-3} [35–38]. Therefore, a low excitation density was used to eliminate the hot-phonon bottleneck effect, and the diffusion measurement was focused on the transport beyond 2 ps to neglect the hot carrier diffusion effects. Here, all the excitation densities for various pump photon energy were around 1.5×10^{17} cm^{-3} which was under the threshold excitation density of the phonon bottleneck effect. Moreover, it is essential to rule out carrier-carrier annihilation effects in transport measurements. If the carrier density at the center of the spot were higher than at the edge, then carrier-carrier annihilation could lead to artificial broadening. We carried out pump fluence dynamics measurements to ensure the impact from annihilation (Fig. S3). It shows similar kinetics with N_0 from 1.5×10^{17} to 9.0×10^{17} cm^{-3}, which suggests that annihilation effects are negligible for the carrier density range here.

To image the carrier transport process, the pump beam was held at a fixed position while the probe beam was scanned relative to the pump with a Galvanometer scanner and ΔT was plotted as a function of probe position. The two-dimensional TAM images are shown in Fig. 3a, b for $MAPbBr_3$ and $CsPbBr_3$ respectively. The initial population was created by a Gaussian pump beam with a pulse duration of ~300 fs. At later delay times, the TAM images reflected carrier diffusing away from the initial excitation volume. It is known that the population follows a Gaussian distribution as a function of delay time t at low excitation intensity where the high-order recombination terms are negligible. The TAM profiles shown in Fig. 3a, b are fitted by two-dimensional Gaussian functions with variances of $\sigma_{t,x}^2$ and $\sigma_{t,y}^2$, where the $\sigma_{t,x}^2$ and $\sigma_{t,y}^2$ are the time-dependent variances of the Gaussian profiles along the x and y axes at delay time t. Because the carrier transport is isotropic, we reduce the problem to 1D and define $\sigma_t^2 = \frac{\sigma_{t,x}^2+\sigma_{t,y}^2}{2}$. The diffusion constant D is then given by $D = \frac{\sigma_{t2}^2-\sigma_{t1}^2}{2(t_2-t_1)}$. Figure 3c, d plot $\sigma_t^2 - \sigma_0^2$ as a function of pump-probe delay time. σ_t^2 grows linearly as a function of delay time t (Fig. 3c, d) as expected for diffusive transport. The carrier diffusion constants of $MAPbBr_3$ and $CsPbBr_3$ were determined to be 0.22 ± 0.02 and 1.68 ± 0.05 cm^2/s respectively by fitting the experimental data. This result is consistent with a previous work, which reveals that the carrier diffusion constants of $CsPbBr_3$ are 4 times higher than that of $MAPbBr_3$ by transient reflection [11].

The diffusion length L is an essential parameter for solar cell materials and can be estimated by the diffusion equation $L = \sqrt{Dt}$, where D is the diffusion coefficient and t is the carrier lifetime. If we calculate the lifetimes from TRPL measurements, the diffusion lengths of $MAPbBr_3$ and $CsPbBr_3$ are about 0.55 and 1.41 μm, respectively. With the replacement of inorganic cations, the stability of perovskites can be improved. Our results show that the carrier diffusion constant and diffusion length of $CsPbBr_3$ also can be boosted compared to $MAPbBr_3$. With these fundamental property measurements, we can illustrate that this may be the probable reason for the excellent photovoltaic performances of $CsPbBr_3$ solar cells, which have similar performances to those of $MAPbBr_3$ solar cells. Large polaron formation has been proposed in hybrid organic–inorganic perovskites, which can effectively screen carrier scattering with optical phonons [39]. For large polaron formation, easy polarization of organic cations with orientational freedom is essential. However, our results show that carriers diffuse faster in all-inorganic $CsPbBr_3$ than hybrid organic–inorganic $MAPbBr_3$, which indicates that remarkable photophysical and transport properties also exist in all-inorganic perovskites. A previous study on elastomechanical properties of $MAPbBr_3$ and $CsPbBr_3$ shows that the organic cation makes the entire structure stiffer compared to inorganic perovskite [39]. Therefore, with the replacement by inorganic cations, the lead halide perovskites are still soft and flexible. The

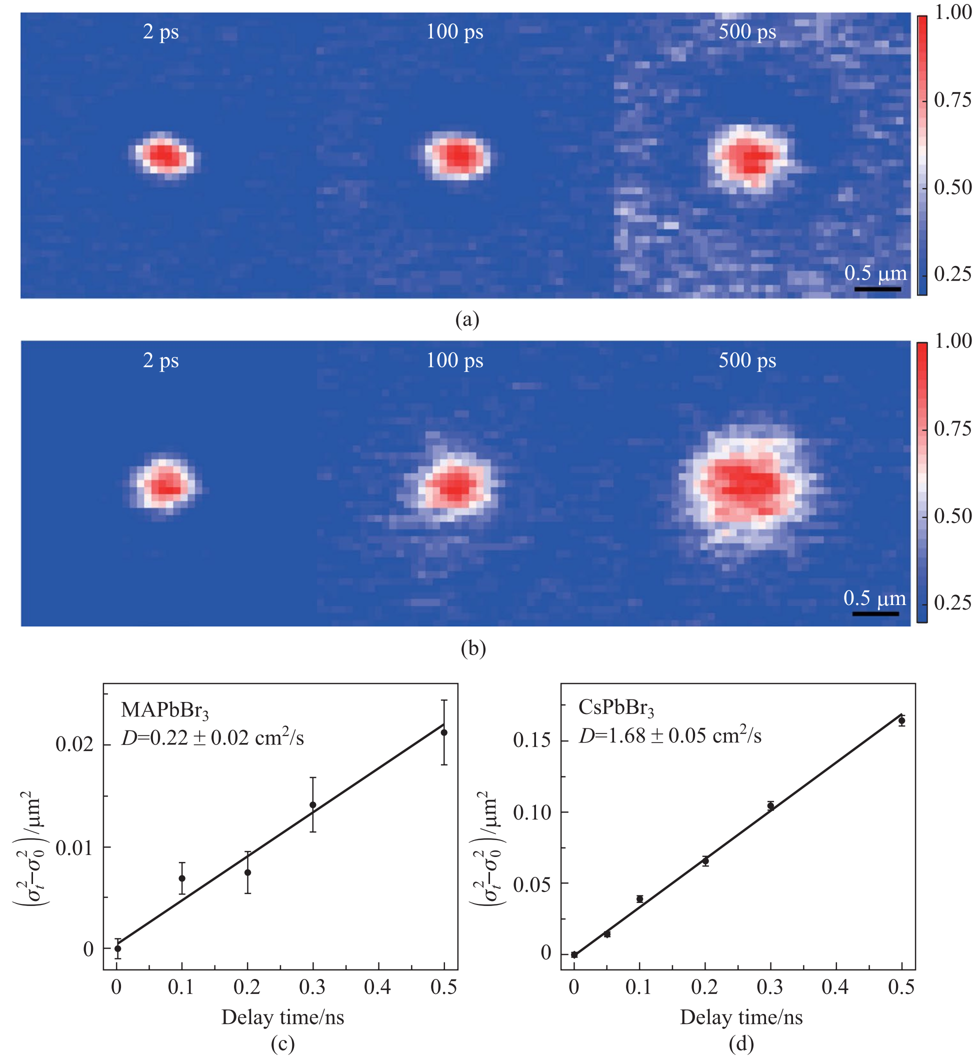

Fig. 3 Carrier diffusion of $MAPbBr_3$ and $CsPbBr_3$. **a** $MAPbBr_3$ and **b** $CsPbBr_3$ TAM images of the carrier transport at various delay times. The color scale represents the intensity of pump-induced differential transmission (ΔT) of the probe and every image has been normalized by peak value. Scale bar: 500 nm. **c** and **d** $\sigma_t^2 - \sigma_{2ps}^2$ plotted as a function of the pump-probe delay time of $MAPbBr_3$ and $CsPbBr_3$, respectively. Solid lines are the linear fits $D = \frac{\sigma_{t2}^2 - \sigma_{t1}^2}{2(t_2 - t_1)}$

soft structure facilitates formation of large polaron which can efficiently screen the carrier scattering with defects and optical phonons regardless of the A-site cation types.

4 Conclusions

In conclusion, this work provides insights into understanding the band edge carrier dynamics and diffusion process of $MAPbBr_3$ and $CsPbBr_3$ single crystal microplates. With the replacement of inorganic cations, both the bulk-free carrier recombination rate and the diffusion constant increase. Besides, the significant property, i.e., diffusion length, is almost 3 times higher than that of $MAPbBr_3$. These results suggest that mixing moderate inorganic Cs^+ cations can enhance the performance of LHP-based devices, not only in structure stability but also in carrier transport. This work reveals an effective way to extend the diffusion length and provides a guide for photovoltaic and other optoelectronics applications of LHP.

Supplementary Information The online version contains supplementary material available at https://doi.org/10.1007/s12200-023-00078-z.

Acknowledgements This work was financially supported by the Ministry of Science and Technology of China (No. 2019YFE0120300), and the Open Project Program of Wuhan National Laboratory for Optoelectronics (No. 2020WNLOKF014).

Author contributions All authors read and approved the final manuscript.

Availability of data and materials The data that support the findings of this study are available from the corresponding author, upon reasonable request.

Declarations

Competing interests The authors declare that they have no competing interests.

References

1. Xing, G., Mathews, N., Sun, S., Lim, S.S., Lam, Y.M., Grätzel, M., Mhaisalkar, S., Sum, T.C.: Long-range balanced electron- and hole-transport lengths in organic-inorganic $CH_3NH_3PbI_3$. Science **342**(6156), 344–347 (2013)
2. Zhao, D., Yu, Y., Wang, C., Liao, W., Shrestha, N., Grice, C.R., Cimaroli, A.J., Guan, L., Ellingson, R.J., Zhu, K., Zhao, X., Xiong, R.G., Yan, Y.: Low-bandgap mixed tin–lead iodide perovskite absorbers with long carrier lifetimes for all-perovskite tandem solar cells. Nat. Energy **2**(4), 17018 (2017)
3. Shi, D., Adinolfi, V., Comin, R., Yuan, M., Alarousu, E., Buin, A., Chen, Y., Hoogland, S., Rothenberger, A., Katsiev, K., Losovyj, Y., Zhang, X., Dowben, P.A., Mohammed, O.F., Sargent, E.H., Bakr, O.M.: Low trap-state density and long carrier diffusion in organolead trihalide perovskite single crystals. Science **347**(6221), 519–522 (2015)
4. Zhumekenov, A.A., Saidaminov, M.I., Haque, M.A., Alarousu, E., Sarmah, S.P., Murali, B., Dursun, I., Miao, X.H., Abdelhady, A.L., Wu, T., Mohammed, O.F., Bakr, O.M.: Formamidinium lead halide perovskite crystals with unprecedented long carrier dynamics and diffusion length. ACS Energy Lett. **1**(1), 32–37 (2016)
5. He, X., Liu, P., Zhang, H., Liao, Q., Yao, J., Fu, H.: Patterning multicolored microdisk laser arrays of cesium lead halide perovskite. Adv. Mater. **29**(12), 1604510 (2017)
6. Sahli, F., Werner, J., Kamino, B.A., Bräuninger, M., Monnard, R., Paviet-Salomon, B., Barraud, L., Ding, L., Diaz Leon, J.J., Sacchetto, D., Cattaneo, G., Despeisse, M., Boccard, M., Nicolay, S., Jeangros, Q., Niesen, B., Ballif, C.: Fully textured monolithic perovskite/silicon tandem solar cells with 25.2% power conversion efficiency. Nat. Mater. **17**(9), 820–826 (2018)
7. Xiao, Z., Kerner, R.A., Zhao, L., Tran, N.L., Lee, K.M., Koh, T.W., Scholes, G.D., Rand, B.P.: Efficient perovskite light-emitting diodes featuring nanometre-sized crystallites. Nat. Photonics **11**(2), 108–115 (2017)
8. Fu, Y., Zhu, H., Chen, J., Hautzinger, M.P., Zhu, X.Y., Jin, S.: Metal halide perovskite nanostructures for optoelectronic applications and the study of physical properties. Nat. Rev. Mater. **4**(3), 169–188 (2019)
9. Kojima, A., Teshima, K., Shirai, Y., Miyasaka, T.: Organometal halide perovskites as visible-light sensitizers for photovoltaic cells. J. Am. Chem. Soc. **131**(17), 6050–6051 (2009)
10. NREL. Available at website of nrel.gov/pv/cell-efficiency.html
11. Zhu, H., Trinh, M.T., Wang, J., Fu, Y., Joshi, P.P., Miyata, K., Jin, S., Zhu, X.Y.: Organic cations might not be essential to the remarkable properties of band edge carriers in lead halide perovskites. Adv. Mater. **29**(1), 1603072 (2017)
12. Etienne, T., Mosconi, E., De Angelis, F.: Dynamical origin of the Rashba effect in organohalide lead perovskites: a key to suppressed carrier recombination in perovskite solar cells? J. Phys. Chem. Lett. **7**(9), 1638–1645 (2016)
13. Motta, C., El-Mellouhi, F., Kais, S., Tabet, N., Alharbi, F., Sanvito, S.: Revealing the role of organic cations in hybrid halide perovskite $CH_3NH_3PbI_3$. Nat. Commun. **6**(1), 7026 (2015)
14. Frost, J.M., Walsh, A.: What is moving in hybrid halide perovskite solar cells? Acc. Chem. Res. **49**(3), 528–535 (2016)
15. Zheng, F., Tan, L.Z., Liu, S., Rappe, A.M.: Rashba spin-orbit coupling enhanced carrier lifetime in $CH_3NH_3PbI_3$. Nano Lett. **15**(12), 7794–7800 (2015)
16. Pecchia, A., Gentilini, D., Rossi, D., Auf der Maur, M., Di Carlo, A.: Role of ferroelectric nanodomains in the transport properties of perovskite solar cells. Nano Lett. **16**(2), 988–992 (2016)
17. Wang, C., Chu, W., Ye, F., Ou, Z., Li, Z., Guo, Q., Zheng, Z., Wang, Z., Liu, X., Fang, G., Prezhdo, O., Wang, T., Xu, H.: Polar methylammonium organic cations detune state coupling and extend hot-carrier lifetime in lead halide perovskites. Chem **8**(11), 3051–3063 (2022)
18. Niu, G., Guo, X., Wang, L.: Review of recent progress in chemical stability of perovskite solar cells. J. Mater. Chem. A Mater. Energy Sustain. **3**(17), 8970–8980 (2015)
19. Wang, S., Zhao, Q., Hazarika, A., Li, S., Wu, Y., Zhai, Y., Chen, X., Luther, J.M., Li, G.: Thermal tolerance of perovskite quantum dots dependent on A-site cation and surface ligand. Nat. Commun. **14**(1), 2216 (2023)
20. Correa-Baena, J.P., Saliba, M., Buonassisi, T., Grätzel, M., Abate, A., Tress, W., Hagfeldt, A.: Promises and challenges of perovskite solar cells. Science **358**(6364), 739–744 (2017)
21. Saliba, M., Matsui, T., Seo, J.Y., Domanski, K., Correa-Baena, J.P., Nazeeruddin, M.K., Zakeeruddin, S.M., Tress, W., Abate, A., Hagfeldt, A., Grätzel, M.: Cesium-containing triple cation perovskite solar cells: improved stability, reproducibility and high efficiency. Energy Environ. Sci. **9**(6), 1989–1997 (2016)
22. Huang, J., Lai, M., Lin, J., Yang, P.: Rich chemistry in inorganic halide perovskite nanostructures. Adv. Mater. **30**(48), e1802856 (2018)
23. Dong, Q., Fang, Y., Shao, Y., Mulligan, P., Qiu, J., Cao, L., Huang, J.: Electron-hole diffusion lengths > 175 μm in solution-grown $CH_3NH_3PbI_3$ single crystals. Science **347**(6225), 967–970 (2015)
24. Xiao, Z., Dong, Q., Bi, C., Shao, Y., Yuan, Y., Huang, J.: Solvent annealing of perovskite-induced crystal growth for photovoltaic-device efficiency enhancement. Adv. Mater. **26**(37), 6503–6509 (2014)
25. Tian, W., Zhao, C., Leng, J., Cui, R., Jin, S.: Visualizing carrier diffusion in individual single-crystal organolead halide perovskite nanowires and nanoplates. J. Am. Chem. Soc. **137**(39), 12458–12461 (2015)

26. Hu, X., Wang, X., Fan, P., Li, Y., Zhang, X., Liu, Q., Zheng, W., Xu, G., Wang, X., Zhu, X., Pan, A.: Visualizing carrier transport in metal halide perovskite nanoplates via electric field modulated photoluminescence imaging. Nano Lett. **18**(5), 3024–3031 (2018)
27. Ou, Z., Wang, T., Tang, J., Zong, X., Wang, W., Guo, Q., Xu, Y., Zhu, C., Wang, L., Huang, W., Xu, H.: Enabling and controlling negative photoconductance of $FePS_3$ nanosheets by hot carrier trapping. Adv. Opt. Mater. **8**(10), 2000201 (2020)
28. Snaider, J.M., Guo, Z., Wang, T., Yang, M., Yuan, L., Zhu, K., Huang, L.: Ultrafast imaging of carrier transport across grain boundaries in hybrid perovskite thin films. ACS Energy Lett. **3**(6), 1402–1408 (2018)
29. Zhu, T., Yuan, L., Zhao, Y., Zhou, M., Wan, Y., Mei, J., Huang, L.: Highly mobile charge-transfer excitons in two-dimensional WS_2/tetracene heterostructures. Sci. Adv. **4**(1), eaao3104 (2018)
30. Chen, J., Fu, Y., Samad, L., Dang, L., Zhao, Y., Shen, S., Guo, L., Jin, S.: Vapor-phase epitaxial growth of aligned nanowire networks of cesium lead halide perovskites ($CsPbX_3$, X=Cl, Br, I). Nano Lett. **17**(1), 460–466 (2017)
31. Zhu, H., Fu, Y., Meng, F., Wu, X., Gong, Z., Ding, Q., Gustafsson, M.V., Trinh, M.T., Jin, S., Zhu, X.Y.: Lead halide perovskite nanowire lasers with low lasing thresholds and high quality factors. Nat. Mater. **14**(6), 636–642 (2015)
32. Tao, S., Schmidt, I., Brocks, G., Jiang, J., Tranca, I., Meerholz, K., Olthof, S.: Absolute energy level positions in tin- and lead-based halide perovskites. Nat. Commun. **10**(1), 2560 (2019)
33. Wu, B., Nguyen, H.T., Ku, Z., Han, G., Giovanni, D., Mathews, N., Fan, H.J., Sum, T.C.: Discerning the surface and bulk recombination kinetics of organic–inorganic halide perovskite single crystals. Adv. Energy Mater. **6**(14), 1600551 (2016)
34. Chung, H., Jung, S.I., Kim, H.J., Cha, W., Sim, E., Kim, D., Koh, W.K., Kim, J.: Composition-dependent hot carrier relaxation dynamics in cesium lead halide ($CsPbX_3$, X=Br and I) perovskite nanocrystals. Angew. Chem. Int. Ed. Engl. **56**(15), 4160–4164 (2017)
35. Yang, Y., Ostrowski, D.P., France, R.M., Zhu, K., van de Lagemaat, J., Luther, J.M., Beard, M.C.: Observation of a hot-phonon bottleneck in lead-iodide perovskites. Nat. Photonics **10**(1), 53–59 (2016)
36. Yang, J., Wen, X., Xia, H., Sheng, R., Ma, Q., Kim, J., Tapping, P., Harada, T., Kee, T.W., Huang, F., Cheng, Y.B., Green, M., Ho-Baillie, A., Huang, S., Shrestha, S., Patterson, R., Conibeer, G.: Acoustic-optical phonon up-conversion and hot-phonon bottleneck in lead-halide perovskites. Nat. Commun. **8**(1), 14120 (2017)
37. Li, M., Bhaumik, S., Goh, T.W., Kumar, M.S., Yantara, N., Grätzel, M., Mhaisalkar, S., Mathews, N., Sum, T.C.: Slow cooling and highly efficient extraction of hot carriers in colloidal perovskite nanocrystals. Nat. Commun. **8**(1), 14350 (2017)
38. Zhu, X.Y., Podzorov, V.: Charge carriers in hybrid organic–inorganic lead halide perovskites might be protected as large polarons. J. Phys. Chem. Lett. **6**(23), 4758–4761 (2015)
39. Rakita, Y., Cohen, S.R., Kedem, N.K., Hodes, G., Cahen, D.: Mechanical properties of $APbX_3$ (A=Cs or CH_3NH_3, X=I or Br) perovskite single crystals. MRS Commun. **5**(4), 623–629 (2015)

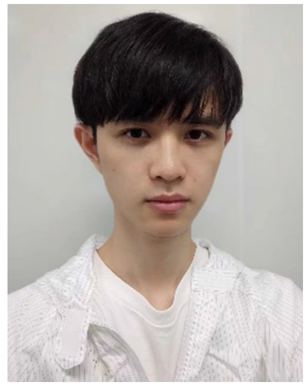

Cheng Wang is a doctoral candidate at Wuhan University, China from 2020 supervised by Prof. Hongxing Xu. His research mainly focuses on carrier dynamics in lead halide perovskite by ultrafast spectroscopy.

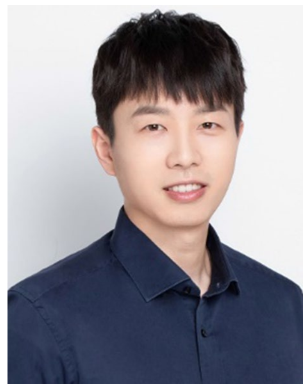

Yaoguang Rong is working as a senior research scientist at Wuhan University of Technology (WUT), China. He received his B.S. degree in Material Physics from Wuhan University, China in 2009, and Ph.D. degree in Optics Engineering from Huazhong University of Science & Technology (HUST), China in 2014. He then worked as a postdoctoral researcher at University of Houston, USA. From 2016 to 2022, he has worked as an associate professor at Wuhan National Laboratory for Optoelectronics at HUST. Since 2023, he has been working at WUT. His research interests focus on emerging photovoltaic technologies (metal halide perovskite solar cells), nano-structured materials and relevant physical dynamics. He has published over 70 peer-review papers (*Science, Nature Energy, Nature Communications, Advanced Materials*, etc.) with citations of over 10,000 times.

Ti Wang is a professor in the School of Physics and Technology at Wuhan University, China. He completed his B.S. degree at Wuhan University in 2007, and later obtained his Ph.D. degree from the same university in 2013. Following his doctoral studies, he pursued postdoctoral research at the University of Kansas and Purdue University, USA. In 2018, he joined the faculty at Wuhan University. His research program centers around studying excited state dynamics in novel semiconductors using pump-probe techniques.